Zero-field spin splitting in a two-dimensional electron gas

B. Das and S. Datta
School of Electrical Engineering, Purdue University, West Lafayette, Indiana 47907

R. Reifenberger
Department of Physics, Purdue University, West Lafayette, Indiana 47907

(Received 26 May 1989)

The spin splitting in zero magnetic field which was recently reported in $In_xGa_{1-x}As/In_{0.52}Al_{0.48}As$ heterostructures is analyzed with use of the inversion-asymmetry, or k^3, term and the interface spin orbit or Rashba term. Comparison with experimental data shows that Rashba term is the dominant spin-splitting mechanism in these samples. Zero-field spin splittings of 2.5–2.75 meV are deduced from the perpendicular-field data. Analysis of tilted-magnetic-field data gives g factors that lie between -2 and -3.

I. INTRODUCTION

In semiconductor heterostructures, the lifting of spin degeneracy in zero magnetic field has attracted much attention lately. Experimentally, the zero-field spin splitting for a two-dimensional electron gas (2D EG) has been investigated in $GaAs/Al_xGa_{1-x}As$ heterostructures only by electron spin resonance (ESR) measurements.[1–3] A very visible manifestation of the zero-field spin splitting is a beating pattern in Shubnikov–de Haas (SdH) oscillations due to two close frequency components with similar amplitudes arising from the spin-split levels. Beating patterns in the SdH oscillations of a 2D EG were reported recently by Luo *et al.* in GaSb-InAs-GaSb quantum wells[4] and by Das *et al.* in $In_xGa_{1-x}As/In_{0.52}Al_{0.48}As$ heterostructures.[5,6] A series of three different $In_xGa_{1-x}As/In_{0.52}Al_{0.48}As$ heterostructures was used in the latter experiment. Two of the samples used were pseudomorphic (sample A, $x=0.65$ and sample B, $x=0.60$) while one was lattice matched (sample C, $x=0.53$).[7] The experimental data in Refs. 5 and 6 shows clear beats with up to six null points in the SdH oscillations for magnetic fields $B<1$ T. The clarity of the beating pattern also made it possible to make measurements by varying the angle of the sample with respect to the applied magnetic field. The purpose of this paper is to analyze this data in order to shed light on the underlying mechanism for the zero-field spin splitting in this material.

In semiconductor heterostructures, two mechanisms are believed to be responsible for producing zero-field spin splitting: (i) a k^3 term related to inversion asymmetry which we will refer to as the I term[8–11] and (ii) a term due to interface spin-orbit interaction which we will refer to as the R term.[11,12] In Sec. II we develop theoretical models for the two mechanisms and compare with the perpendicular-field experimental data. Neglecting the I term and considering only the R term, we obtain an analytical expression for the spin splitting as a function of $\hbar\omega_c$ which matches the experimental data very well. The agreement deteriorates significantly if we assume an I term comparable in strength to the R term or consider the I term alone. An approximate theoretical estimate also indicates that the matrix elements due to the R term are 30–100 % larger than those due to the I term. From this we conclude that the R term is the dominant spin-splitting mechanism in these samples and that the I term can be neglected. This leads to a simple and convenient model in contrast to the more complex numerical analysis that is necessary in general.[11] In Sec. III from comparison of the tilted field data with the theoretical model we deduce g factors that lie between -2 and -3 in these materials. The conclusions are summarized in Sec. IV.

II. SPIN SPLITTING IN PERPENDICULAR MAGNETIC FIELD

A. Theory

In semiconductor heterostructures, the two mechanisms responsible for lifting the spin degeneracy of conduction-band electrons are the inversion-asymmetry or k^3 term and the interface spin-orbit or Rashba term. The Hamiltonian for a 2D EG (in the x-y plane) with a confining potential $V(z)$ in a uniform magnetic field $\mathbf{B}$ is written as

$$H=H_0+H_I+H_R \tag{1}$$

where

$$H_0=\frac{\hbar^2k^2}{2m^*}+g\mu_B\boldsymbol{\sigma}\cdot\mathbf{B}+V(z)\ , \tag{2}$$

$$H_I=\gamma\boldsymbol{\sigma}\cdot\boldsymbol{\kappa}\ , \tag{3}$$

$$H_R=\eta[\boldsymbol{\sigma}\times\mathbf{k}]\cdot\hat{\mathbf{z}}\ , \tag{4}$$

$$\hbar\mathbf{k}=\mathbf{p}+e\,\mathbf{A}\ . \tag{5}$$

γ is the inversion asymmetry parameter; σ_x, σ_y, σ_z are the Pauli spin matrices; η is the spin-orbit-coupling con-

stant; m^* is the effective mass; μ_B is the Bohr magneton; g is the g factor; $\mathbf{p}$ is the momentum operator, and $\mathbf{A}$ is the vector potential corresponding to the magnetic field. The vector $\boldsymbol{\kappa}$ is given by Eq. (A1) in Appendix A. The k-dependent contributions to g factor, important in ESR measurements,[2] are not included in Eq. (1) for the following reason. The spin splitting in Ref. 5 is obtained from SdH measurements, and as shown in Appendix B, in such measurements the k-dependent contributions introduce a constant correction to the g factor that does not change with magnetic field. Hence, in our case, this term is not expected to introduce nonlinearity in the magnetic field dependence of the spin splitting. This is discussed in more detail in Appendix B. We assume that the magnetic field $\mathbf{B}$ is in the $\hat{\mathbf{z}}$ direction. The Hamiltonian H_0 is exactly solvable and we will use the eigenstates of H_0 as the basis set and treat H_I and H_R as perturbations. The eigenstates of H_0 can be written as $|\alpha,n,s\rangle$ where α is the subband index, n is the Landau index, and s is the spin index. The energy eigenvalues of H_0 are given by (Appendix A)

$$E(\alpha,n,s)=E_\alpha+\hbar\omega_c\left[n+\frac{1}{2}+\frac{\nu_0}{2}s\right] \tag{6}$$

where $\omega_c=eB/m^*$ and $\nu_0=gm^*/2m_0$. This is the well-known result for the Landau levels of conduction-band electrons. To find the effects of H_I and H_R we need to evaluate the matrix elements $\langle\alpha,n,s|H_I|\alpha',n',s'\rangle$ and $\langle\alpha,n,s|H_R|\alpha',n',s'\rangle$ between the eigenstates of H_0. We restrict ourselves to the lowest subband ($\alpha=\alpha'=1$) and neglect any intersubband mixing. It is shown in Appendix A that the inversion-asymmetry term H_I leads to the matrix elements Δ_I and $\Delta_{I'}$ while the Rashba term H_R leads to the matrix element Δ_R (Fig. 1); the matrix elements Δ_I, $\Delta_{I'}$, and Δ_R are given in Eqs. (A21a), (A21b), and (A25), respectively. It may be noted that a uniaxial strain along z direction can produce a perturbation similar to H_1 [Eq. (A11)] in Appendix A. The samples investigated have a wide range of strains (intended or unintended) but show similar zero-field spin splittings. This indicates that strain is not the dominant spin-splitting mechanism and is ignored in this analysis. The magnitudes of the matrix elements depend on material as well as heterostructure parameters. Following the procedure outlined below, we have theoretically estimated the matrix elements and obtained $\Delta_{I,\text{theor}}\simeq 0.26$ meV, $\Delta_{I',\text{theor}}\simeq 0.37$ meV, and $\Delta_{R,\text{theor}}\simeq 0.48$ meV. The conduction-band discontinuity ΔE_c was adjusted to match the experimentally determined 2D EG carrier density; the ΔE_c required was $0.69\,\Delta E_g$. On the other hand, if we assume $\Delta E_c=0.57\,\Delta E_g$, which is more commonly used, we obtain $\Delta_{I,\text{theor}}\simeq 0.22$ meV, $\Delta_{I',\text{theor}}\simeq 0.29$ meV, and $\Delta_{R,\text{theor}}\simeq 0.43$ meV.

The estimation of Δ_I and $\Delta_{I'}$ requires the inversion-asymmetry parameter γ which was calculated following the procedure in Ref. 11. From extrapolated material parameters we obtained $\gamma\simeq -44$ eV Å^3 for this system and from Eq. (A21b) we obtained $\Delta_{I',\text{theor}}\simeq 0.37$ meV. To calculate Δ_I we also need K^2 (Eq. A12) which was estimated by obtaining the wave functions in the heterostructures in the following manner. First, the band diagram for each heterostructure was obtained by using the technique described in Ref. 13. Material parameters used in the calculations are shown in Table I. The conduction-band discontinuity ΔE_c was adjusted to match the experimentally determined 2D EG carrier density; the ΔE_c required was $0.69\,\Delta E_g$ which is within the range reported in the literature.[17,18] Next, the subband energy levels and the corresponding wave functions in the heterostructures were obtained by following the method described in Ref. 19. The effective well width confining the 2D EG was then obtained by matching the calculated wave function to the ground-state wave function of a rectangular infinite potential well of width w. K^2 was then calculated from Eq. (A12) and we obtained $\Delta_{I,\text{theor}}\simeq 0.26$ meV. The estimation of Δ_R [Eq. (A25)] requires the spin-orbit-coupling constant η which is the product of a material-specific coefficient a_{46} (Ref. 11) and the expectation value of the electric field in the heterostructure. Following the procedure in Ref. 11, we obtained $a_{46}\simeq 30$ C Å^2. Using the ground-state wave function and the potential distribution in the heterostructures, the expectation value of the electric field was $\simeq 0.49\times 10^7$ V/m for samples A and B which led to $\eta\simeq 1.46\times 10^{-12}$ eV m and $\Delta_{R,\text{theor}}\simeq 0.48$ meV. In these samples we thus obtain $\Delta_R\simeq 1.8\,\Delta_I$ and $1.3\,\Delta_{I'}$. The values quoted above should be regarded as approximate because of the uncertainties involved in the estimation of material constants, K^2, and the expectation value of the electric field.

The theoretical estimates show that in these samples Δ_R is larger than Δ_I and $\Delta_{I'}$, which is to be expected in narrow band-gap materials.[4,11] If we neglect Δ_I and $\Delta_{I'}$, the problem is simplified considerably since the matrix element Δ_R couples the energy levels in pairs (Fig. 1). We show in the next section that the R term (Δ_R) alone can explain the experimental data very well. We also show that the agreement with the experimental data deteriorates significantly if we assume an I term comparable in strength to the R term or consider the I term alone. This suggests that the R term is the dominant spin-splitting mechanism in these samples and that the I term can be neglected. Considering only Δ_R, the new energy levels can be obtained in a straightforward manner[12] by diagonalizing a 2×2 matrix and the spin splitting δ is given by

$$|\delta|=\{[(1-\nu_0)\hbar\omega_c]^2+(2\Delta_R)^2\}^{1/2}-\hbar\omega_c\simeq\begin{cases}2|\Delta_R|-\hbar\omega_c & \text{if } \hbar\omega_c\ll\dfrac{2|\Delta_R|}{1-\nu_0}\\ |\nu_0|\hbar\omega_c & \text{if } \hbar\omega_c\gg\dfrac{2|\Delta_R|}{1-\nu_0}\end{cases}. \tag{7}$$

TABLE I. $In_xGa_{1-x}As$ and $In_{0.52}Al_{0.48}As$ parameters used for calculating band diagrams.

Material parameter	$In_xGa_{1-x}As$	$In_{0.52}Al_{0.48}As$
Direct energy gap, E_g (eV)	$1.52-1.602x+0.502x^2$ [a]	1.508[b]
Effective mass, m^*/m_0	0.046[c]	0.076[d]
Dielectric constant	$13.1+1.5x$ [e]	12.42[f]
Donor level (meV)		15[f]

[a]Obtained for $T=0$ K by taking a similar expression for E_g at $T=300$ K (Ref. 14) and calculating the coefficients from known band gaps for In As, GaAs, and $In_{0.53}Ga_{0.47}As$ at $T=0$ K.
[b]Reference 15.
[c]Reference 7.
[d]Reference 16.
[e]Reference 14.
[f]Reference 17.

The result [Eq. (7)] can be understood as follows. As $B\rightarrow 0$ (Fig. 2), the unperturbed energy levels coupled by Δ_R are almost degenerate, and the effect of the coupling is strongest. Each down-spin energy level is increased by Δ_R and each up-spin level is decreased by Δ_R. The spin splitting as $B\rightarrow 0$ is thus $2\Delta_R$ which is also predicted from Eq. (7). At large magnetic fields, the unperturbed levels coupled by Δ_R are separated far apart in energy. Due to this, the effect of the coupling is significantly reduced and the spin splitting δ [Eq. (7)] approaches Zeeman splitting. It may be noted from Eq. (7) that, at low magnetic fields, the spin splitting decreases linearly with $\hbar\omega_c$. The slope, however, does not represent Zeeman splitting alone and cannot be used to obtain the g factor. At high magnetic fields, Zeeman splitting dominates, and the slope can be used to estimate g factor. In this work, the experimental data are at low magnetic fields and it is only by analyzing the spin splitting in a tilted magnetic field that we obtain the g factor.

It will be noted that the sign of the splitting is ambiguous. This is because the energy levels are mixed states of up and down spins. From Fig. 2, the couplings produced by the matrix element Δ_R mix the different eigenstates of H_0. As shown before, the eigenstates of H_0 are spin-split (Zeeman splitting) Landau levels, with up and down spins defined along the z axis. As a result of the mixing, the final states produced are mixtures of the different spin-split Landau levels linked by the matrix elements. These final states thus cannot be labeled by single Landau indices. Also, the spin states of these final levels are mixtures of both up and down spins. Thus, what we refer to as "spin splitting" for lack of a better name, cannot be defined as the energy separation between pure up- and down-spin states of a single Landau level, which is the more traditional definition of spin splitting. The final states can be separated into two groups of energy levels, with $\hbar\omega_c$ as the energy separation within each group. What spin splitting actually represents is the energy separation between these two groups of levels, which in the limit of $B\rightarrow 0$ is the zero-field spin splitting. Also, since these final states are mixtures of both spins, the sign of the spin splitting, as well as the zero-field spin splitting, is not well defined.

B. Comparison with experiment

In the experiment with the magnetic field perpendicular to the 2D EG plane, the spin splittings as a function

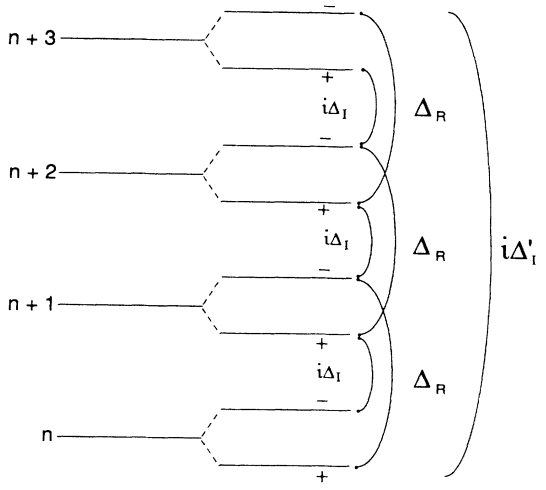

FIG. 1. Unperturbed energy levels of H_0 and the couplings introduced by the matrix elements Δ_I, $\Delta_{I'}$ and Δ_R.

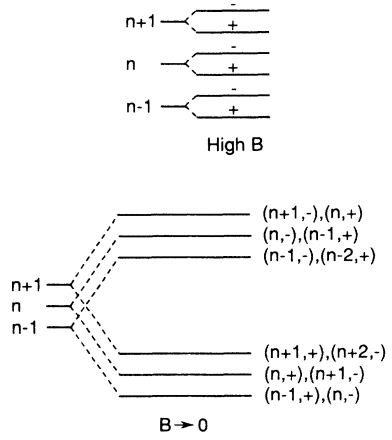

FIG. 2. Unperturbed energy levels of H_0 and perturbed energy levels for large B and as $B\rightarrow 0$.

of $\hbar\omega_c$ were obtained for the three samples from the locations of the null points.[5,6] We have used Eq. (7) to fit the experimental data with Δ_R as the fitting parameter. We concentrate on samples A and B since each of them has six null points. The g factor needed in Eq. (7) is not known for the following reasons. Samples A and B are pseudomorphic strained structures which are relatively new and not well understood. Also, because of the zero-field spin splitting, there is a possibility for the g factor to be enhanced. We have used two different values of g factors, the bulk value of -3 in $In_{0.53}Ga_{0.47}As$, and an enhanced value of -8 measured in $In_{0.53}Ga_{0.47}As/In_{0.52}Al_{0.48}As$ heterostructures[20] for the range of spin splitting observed in the samples in Ref. 5. The results using the two g factors for sample A are shown in Figs. 3(a) and 3(b). The results for sample B are shown in Figs. 4(a) and 4(b). The quality of the fit to the experimental data was very sensitive to Δ_R but not very sensitive to g factor, particularly in the low-field range where most of the data points are. From Figs. 3 and 4 it can be seen that the data for both the samples can be explained very well by the analytical expression for spin splitting for the R term. The values of Δ_R obtained from the theoretical fits have uncertainties of ± 0.2 meV. Comparison of the matrix elements required to fit the experimental data with the theoretically estimated values show that they are in good agreement with $\Delta_{R,\text{expt}} \simeq 2.6\,\Delta_{R,\text{theor}}$.

We have seen that the experimental data is explained very well by the R term (Δ_R) alone, and neglecting the I term (Δ_I and $\Delta_{I'}$). Next, we consider the cases when the I term only is present and both the I and the R terms are present, and compare with the experiment. For these cases we have numerically calculated the spin splitting as a function of $\hbar\omega_c$ using the theoretically estimated values of the matrix elements. The calculation procedure will be discussed in Sec. III. The results of the calculations are shown in Fig. 5, where $\delta/\hbar\omega_c$ is plotted as a function of $1/\hbar\omega_c$ for the cases (i) $\Delta_R = 0.48$ meV, $\Delta_I = \Delta_{I'} = 0$, (ii) $\Delta_R = 0$, $\Delta_I = 0.26$ meV, and $\Delta_{I'} = 0.37$ meV, and (iii) $\Delta_R = 0.48$ meV, $\Delta_I = 0.26$ meV, and $\Delta_{I'} = 0.37$ meV. For case (i), the spin splitting changes monotonically with $\hbar\omega_c$ and null points in SdH oscillations occur when $\delta/\hbar\omega_c = 0.5$, 1.5, 2.5, etc. For cases (ii) and (iii), Fig. 5 shows that δ does not change monotonically with $\hbar\omega_c$. For case (ii) the null locations occur when $\delta/\hbar\omega_c = 0.5$, 1.5, 2.5, etc. whereas for case (iii), the highest-field null

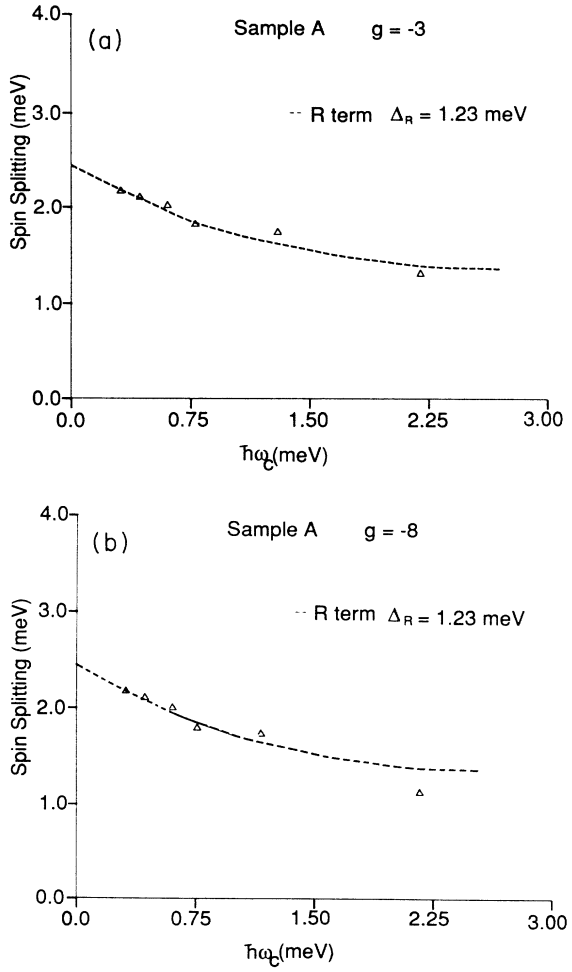

FIG. 3. Experimental spin splittings as a function of $\hbar\omega_c$ for sample A (Ref. 5) and theoretical fit using the R term with (a) $g = -3$ and (b) $g = -8$.

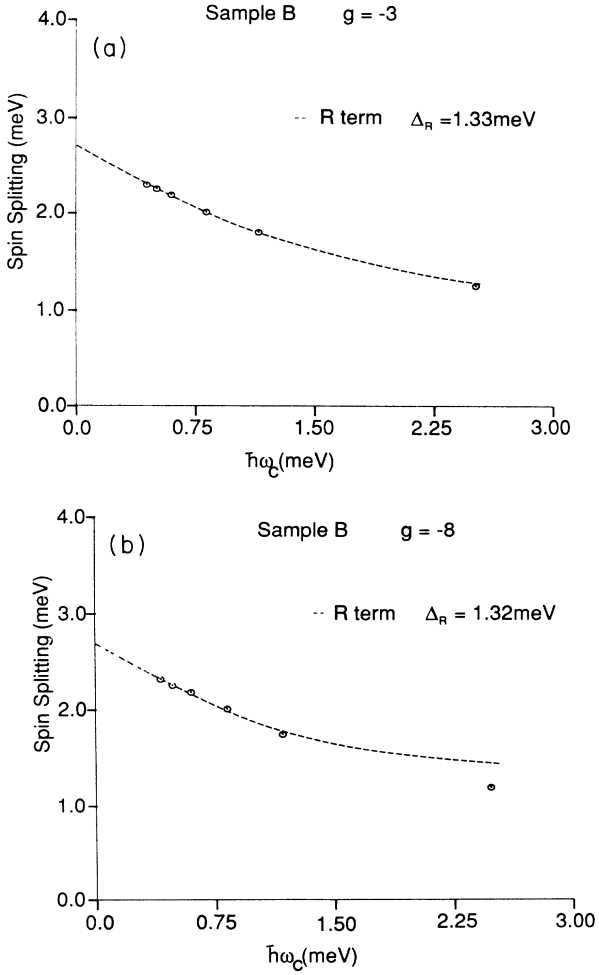

FIG. 4. Experimental spin splitting as a function of $\hbar\omega_c$ for sample B (Ref. 5) and theoretical fit using the R term with (a) $g = -3$ and (b) $g = -8$.

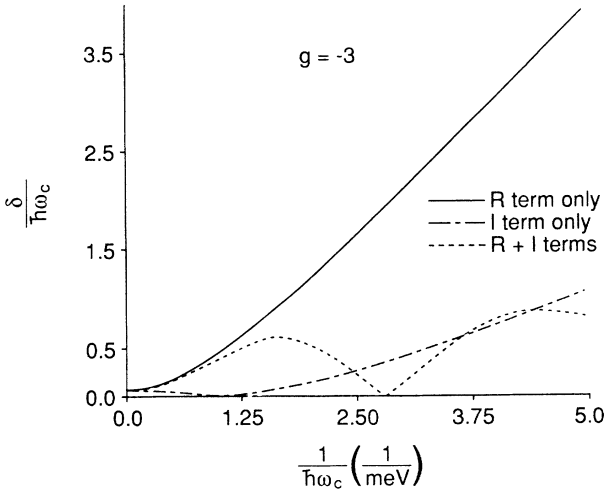

FIG. 5. $\delta/\hbar\omega_c$ vs $1/\hbar\omega_c$ for (i) $\Delta_R=0.48$ meV, $\Delta_I=\Delta_{I'}=0$, (ii) $\Delta_R=0$, $\Delta_I=0.26$ meV, and $\Delta_{I'}=0.37$ meV, and (iii) $\Delta_R=0.48$ meV, $\Delta_I=0.26$ meV, and $\Delta_{I'}=0.37$ meV.

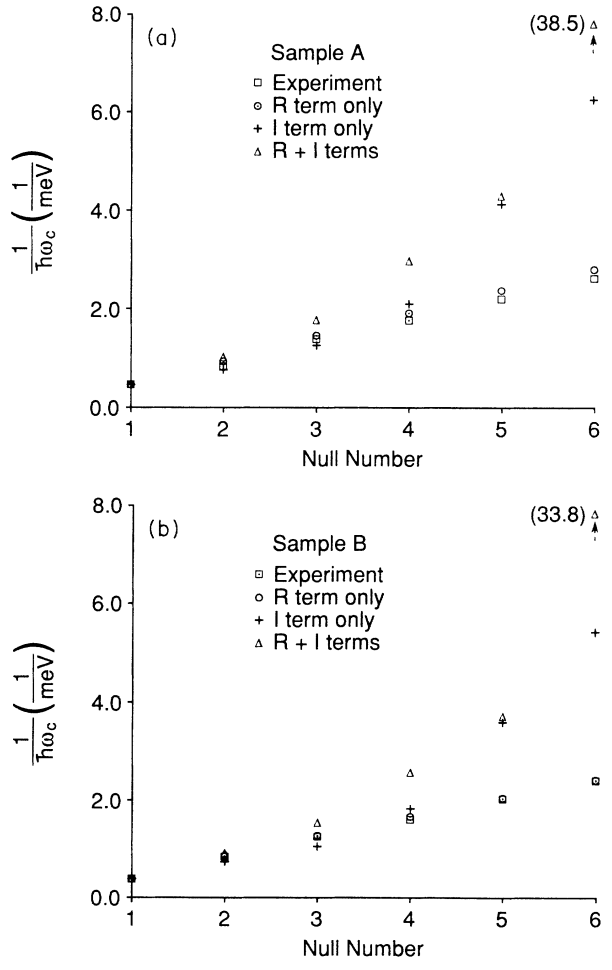

FIG. 6. Comparison of experimental null locations from Ref. 5 with cases (i), (ii), and (iii) defined in the caption for Fig. 5 for (a) sample A and (b) sample B.

points all occur at the same value of $\delta/\hbar\omega_c=0.5$. We should take this into account if we were to translate the experimental null locations into a plot of spin splittings as was done earlier.[5] Instead, we have decided to compare the null locations directly with the theory. In the experiment, six null points in samples A and B were observed. We compare the experimental null locations with those predicted for cases (ii) and (iii). For a comparison, we also perform the same analysis for case (i). The experimental null locations and comparison with the three cases are shown in Fig. 6(a) for sample A and in Fig. 6(b) for sample B. For case (i), Δ_R was adjusted to match the highest-field null point. For cases (ii) and (iii), Δ_I was adjusted to match the highest-field null point, and the other matrix elements were chosen in the same proportion as predicted theoretically. From Fig. 6 it is clear that the null locations for cases (ii) and (iii) do not agree well with the experiment. For case (i) with Δ_R only present, as expected, the null locations agree well with the experiment. However, the match with the experimental data in Fig. 6(a) is not as good as in Fig. 3(a). This is because in Fig. 3(a), Δ_R was adjusted to fit the low-field data points, while in Fig. 6(a), Δ_R was adjusted to match the last null point. From Figs. 6(a) and 6(b) it is seen that the experimental null locations are predicted very well by the R term alone, and not as well when only the I term or when both the I and the R terms are present. This confirms that R term is the dominant zero-field spin-splitting mechanism in these materials.

III. SPIN SPLITTING IN TILTED MAGNETIC FIELD

For a 2D EG, the energy separation between the Landau levels is determined only by the component of magnetic field perpendicular to the 2D EG layer, whereas the Zeeman splitting depends on the total magnetic field applied. By tilting the magnetic field, it is possible therefore to separately adjust the Zeeman splitting and the Landau level separation. This tilted field technique was first applied by Fang and Stiles to measure g factors in Si inversion layers,[21] and since has been widely used to study spin-related effects in two-dimensional systems. In the tilted field method, level coincidences, that is evenly spaced ladders of spin and Landau split levels, are produced which are then detected by their influence on the form of the SdH oscillations. Careful measurements are necessary to precisely determine the angle at which coincidence occurs; from this the g factors are calculated.

In the $In_xGa_{1-x}As/In_{0.52}Al_{0.48}As$ samples, the clarity of the beating pattern made it possible to make measurements by varying the angle of the sample with respect to the applied magnetic field, allowing the spin splitting to be adjusted by the total field while the SdH oscillations are only affected by the component of B perpendicular to the 2D EG.[5] Since the beats are influenced by the total spin splitting, the locations of the nulls were expected to move to higher magnetic fields whenever $g\mu_B B_{\rm tot}$ became comparable to zero-field splitting. Experimentally the locations of the last three nulls were measured as a function of magnetic field as samples A and B were tilted. As ex-

pected, the beat positions scaled as $\cos\theta$ for small angles θ, but steeply increased after a critical angle. Since this steep rise is observed when the Zeeman splitting becomes comparable to the zero-field splitting, an analysis of this data is expected to provide the g factors in these materials. An advantage of this technique is that no precise determination of conditions like level coincidences is required. The theory for spin splitting in a tilted magnetic field with Δ_R as the dominant zero-field spin-splitting term is developed in Sec. III A and the procedure for numerical calculations is discussed. In Sec. III B we compare the theoretical results with the experimental data for samples A and B and obtain g factors for the two samples.

A. Theory

A magnetic field applied at an angle θ to the 2D EG layer can be separated into a perpendicular and a parallel component. The theory for the perpendicular field has been discussed in detail in Sec. II and in Appendix A. The parallel component of the field B_x introduces an additional term $H_{B\parallel}$ in the effective-mass Hamiltonian in Eq. (1) given by

$$H_{B\parallel}=\tfrac{1}{2}g\mu_B\begin{bmatrix}0 & B_x\\ B_x & 0\end{bmatrix}. \tag{8}$$

Noting that $g\mu_B B_\perp=\nu_0\hbar\omega_c$, Eq. (8) can be written as

$$H_{B\parallel}=\xi\begin{bmatrix}0 & 1\\ 1 & 0\end{bmatrix} \tag{9}$$

where $\xi=\hbar\omega_c(\nu_0/2)\tan\theta$.

It is clear from Eq. (9) that $H_{B\parallel}$ couples the up and down spins of the same Landau level. The parallel component of the field thus introduces additional coupling between the eigenstates of H_0. Figure 7 schematically shows the unperturbed energy levels of H_0 and the couplings produced by the parallel field component and Δ_R.

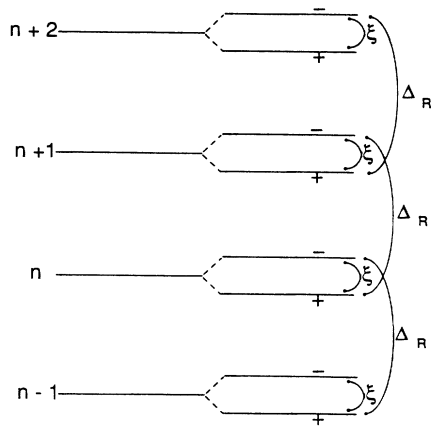

FIG. 7. Couplings introduced by the parallel field component and Δ_R.

The solution of the problem now involves writing down the matrix, and then solving for the eigenvalues. We have numerically calculated the eigenvalues and obtained $B_\perp$ as a function of θ. The procedure for calculation is briefly outlined below.

Calculations started with the assumption of a g factor. Negative values of g were assumed, in agreement with the sign of g determined in $In_{0.53}Ga_{0.47}As/In_{0.52}Al_{0.48}As$.[20] The values of Δ_R for the two samples were chosen from fitting of the perpendicular-field data (Sec. II). Then, for each value of θ, the spin splitting δ as a function of $\hbar\omega_c$ was obtained by numerically calculating the eigenvalues. The matrix was chosen large enough that further increasing its size did not affect the results. A problem encountered, common in numerical solution of eigenvalue problems, was to keep track of the different energy eigenvalues, particularly during energy-level crossovers. This problem was solved by tracking a pair of known eigenvectors. As $\hbar\omega_c$ was changed, the eigenvectors were tracked by finding the new eigenvector with the largest component along the known eigenvector. At each step the known eigenvector was replaced by the new one. The eigenvalues of the tracked eigenvectors were used to calculate δ.

To calculate $B_\perp$, it may be noted that null points occur when $\delta/\hbar\omega_c=0.5$, 1.5, etc.[5] For small angles θ, $\delta/\hbar\omega_c$ changes monotonically with $\hbar\omega_c$, and $B_\perp$ was obtained from the values of $\hbar\omega_c$ for which $\delta/\hbar\omega_c=0.5$ for the last (highest-field) null point, $\delta/\hbar\omega_c=1.5$ for the second last null point, and $\delta/\hbar\omega_c=2.5$ for the third last null point. For large θ, the coupling from the parallel field component becomes stronger, and $\delta/\hbar\omega_c$ no longer changes monotonically with $\hbar\omega_c$. This is shown in Fig. 8 for $\theta=0°$ and 70° where $\delta/\hbar\omega_c$ is plotted as a function of $\Delta_R/\hbar\omega_c$. For large θ, $B_\perp$ for the lower-field null points are obtained for $\delta/\hbar\omega_c=0.5$. This was repeated for different values of θ, and for each value of g factor, a plot of $B_\perp$ as a function of θ was generated. The g factors for the samples were obtained by matching the theoretical plots with the experimental data of $B_\perp$ as a function of θ. A more detailed discussion of the calculation procedure is presented in Ref. 6.

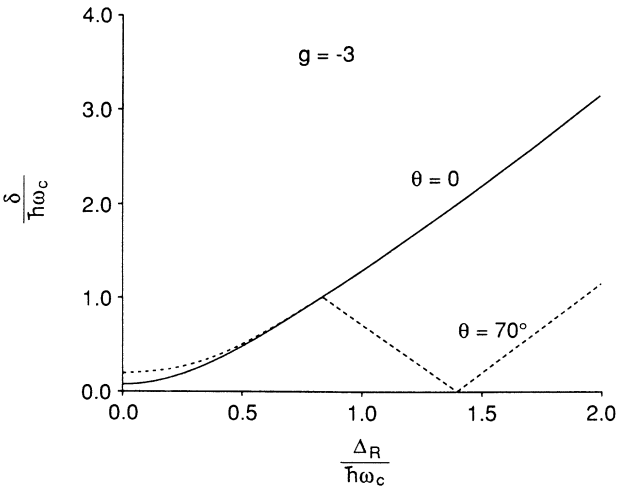

FIG. 8. $\delta/\hbar\omega_c$ as a function of $\Delta_R/\hbar\omega_c$ for $\theta=0°$ and 70°.

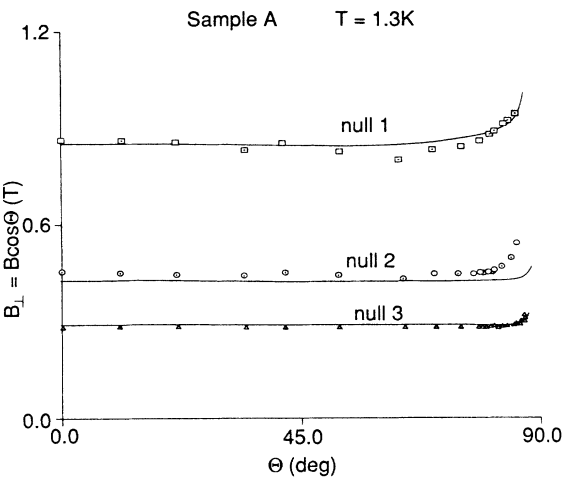

FIG. 9. Tilted-magnetic-field data for sample A (Ref. 5) and theoretical fit with $g=-2.2$.

B. Comparison with experiment

From the experiment, $B_\perp$ remains constant for low angles and then increases rapidly after a critical angle. Our calculations show a similar dependence and also show that the critical angle is very sensitive to the value of g factor chosen, but not sensitive to Δ_R. The experimental data for samples A and B (Refs. 5 and 6) and the theoretical plots are shown in Figs. 9 and 10, which show good agreement. The g factors obtained for samples A and B are -2.2 and -2.8, respectively. From Fig. 10, the uncertainty in the g factor is estimated to be ± 0.1. For sample A, the obtained Δ_R from the last null in the tilted field data was 1.14 meV rather than 1.23 meV obtained from the perpendicular-field data. This lower value of Δ_R required can be understood from Fig. 3(a), where it may be noted that the data corresponding to the last null point do not agree well with the theoretical plot. The g factors obtained for samples A and B are close to the bulk $In_{0.53}Ga_{0.47}As$ value of -3 and no enhancement has been observed. The effect of k-dependent contributions to g factor (see Appendix B), not included in this model, can change the values of g factors estimated.

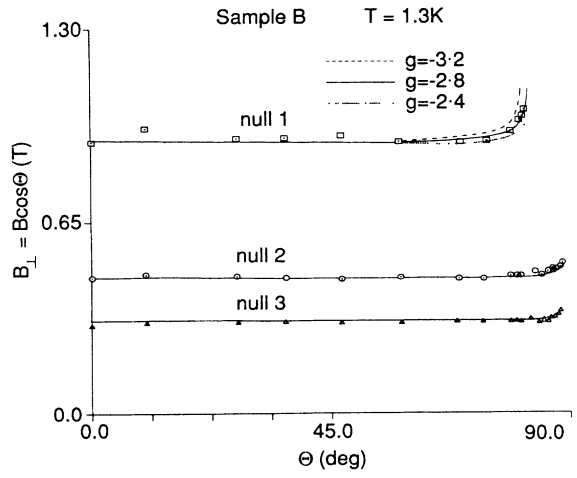

FIG. 10. Tilted-magnetic-field data for sample B (Ref. 6) and theoretical fit with $g=-2.4$, -2.8, and -3.2.

IV. CONCLUSIONS

The zero-field spin splitting as observed from beating effects in the SdH oscillations in $In_xGa_{1-x}As/In_{0.52}Al_{0.48}As$ heterostructures[5] were investigated using the interface-spin-orbit interaction (R term) and inversion-asymmetry splitting (I term). The conclusion is that the R term is the dominant spin-splitting mechanism in these samples. From the perpendicular-field data we obtained zero-field spin splittings of 2.5–2.75 meV for the two samples investigated. The tilted field data are explained very well by the R term and give negative g factors that lie between -2 and -3 for these samples.

ACKNOWLEDGMENTS

This work was supported by the National Science Foundation (NSF) under Grant No. ECS-83-51036 (B.D.), by NSF Division of Materials Research Grant No. DMR-85-2086A2 (S.D.), and by NSF Grant No. DMR-86-10368 (R.R.). The authors would like to acknowledge S. Rodriguez (Purdue University) and P. K. Bhattacharya and J. Singh (University of Michigan) for helpful discussions.

APPENDIX A: MATRIX ELEMENTS OF H_I AND H_R

In this appendix we obtain the eigenstates of H_0 [Eq. (2) and compute the matrix elements for H_I [Eq. (3)] and H_R [Eq. (4)]. The vector $\boldsymbol{\kappa}$ in Eq. (3) is given by[22,23]

$$\kappa_x=\tfrac{1}{2}[k_x(k_y^2-k_z^2)+(k_y^2-k_z^2)k_x]\ , \tag{A1a}$$

$$\kappa_y=\tfrac{1}{2}[k_y(k_z^2-k_x^2)+(k_z^2-k_x^2)k_y]\ , \tag{A1b}$$

$$\kappa_z=\tfrac{1}{2}[k_z(k_x^2-k_y^2)+(k_x^2-k_y^2)k_z]\ . \tag{A1c}$$

From Eq. (5) it can be shown that

$$\mathbf{k}\times\mathbf{k}=-ie\mathbf{B}/\hbar\ . \tag{A2}$$

Assuming the magnetic field $\mathbf{B}$ to be in the z direction, the vector potential in the symmetric gauge is written as

$$\mathbf{A}=(-By/2,Bx/2,0)\ . \tag{A3}$$

Introducing the creation and annihilation operators

$$a=\sqrt{\hbar/2eB}\,(ik_x+k_y)\ , \tag{A4a}$$

$$a^\dagger=\sqrt{\hbar/2eB}\,(-ik_x+k_y)\ , \tag{A4b}$$

we can write H_0 [Eq. (2)] as

$$H_0=\hbar\omega_c(a^\dagger a+\tfrac{1}{2})+\nu_0\hbar\omega_c\sigma_z+H_z \tag{A5}$$

where

$$\nu_0=gm^*/2m_0\ , \tag{A6a}$$

$$\omega_c=eB/m^*\ , \tag{A6b}$$

and

$$H_z=\frac{p_z^2}{2m^*}+V(z)\ , \tag{A7}$$

The eigenfunctions of H_0 can be written as $|\alpha,n,s\rangle$ where α is the subband index

$$H_z|\alpha\rangle=\varepsilon_\alpha|\alpha\rangle\ , \tag{A8a}$$

n is the Landau index

$$a^\dagger a|n\rangle=n|n\rangle\ , \tag{A8b}$$

and s is the spin index (±1)

$$\sigma_z|s\rangle=s|s\rangle\ . \tag{A8c}$$

The energy eigenvalue $E(\alpha,n,s)$ is given by

$$E(\alpha,n,s)=\varepsilon_\alpha+\hbar\omega_c\left[n+\tfrac{1}{2}+\frac{\nu_0}{2}s\right]\ . \tag{A9}$$

These are the well-known results for the Landau levels of conduction electrons in a spherical band. We will now consider the effect of the inversion-asymmetry splitting term H_I [Eq. (3)].

We need to evaluate the matrix elements $\langle\alpha,n,s|H_I|\alpha',n',s'\rangle$ due to H_I between the eigenstates of H_0. We will restrict ourselves to the lowest subband ($\alpha=\alpha'=1$) and neglect any intersubband mixing. We can write from Eqs. (3) and (A1) (note that $\langle1|k_z|1\rangle=0$)

$$\langle\alpha=1|H_I|\alpha'=1\rangle=H_1+H_2 \tag{A10}$$

where

$$H_1=\gamma K^2(\sigma_y k_y-\sigma_x k_x)\ , \tag{A11}$$

$$K^2=\langle1|k_z^2|1\rangle=\frac{\langle1|p_z^2|1\rangle}{\hbar^2}\sim\left[\frac{\pi}{w}\right]^2\ , \tag{A12}$$

$$H_2=\gamma\left[\frac{\sigma_x}{2}(k_x k_y^2+k_y^2 k_x)-\frac{\sigma_y}{2}(k_y k_x^2+k_x^2 k_y)\right]\ , \tag{A13}$$

K^2 is a measure of the kinetic energy in the z direction due to the surface confinement, and w is the effective width of the potential well confining the electrons. Using Eq. (A2) we can write H_2 in Eq. (A13) as

$$H_2=\gamma(\sigma_x k_y k_x k_y-\sigma_y k_x k_y k_x)\ . \tag{A14}$$

To evaluate the matrix elements $\langle n,s|H_{1,2}|n',s'\rangle$ we write H_1 and H_2 in terms of the creation and annihilation operators using Eqs. (A4). We obtain

$$H_1=\gamma K^2\left[\frac{2eB}{\hbar}\right]^{1/2}\begin{bmatrix}0 & -ia^\dagger\\ ia & 0\end{bmatrix} \tag{A15}$$

and

$$H_2=\frac{\gamma}{4}\left[\frac{2eB}{\hbar}\right]^{3/2}\begin{bmatrix}0 & ia^\dagger aa^\dagger-ia^3\\ -iaa^\dagger a+ia^{\dagger3} & 0\end{bmatrix}\ . \tag{A16}$$

It is now straightforward to write down the matrix elements. The only nonzero matrix element of H_1 is

$$\langle n-1,-|H_1|n,+\rangle=i\gamma K^2\left[\frac{2eBn}{\hbar}\right]^{1/2} \tag{A17}$$

while the nonzero matrix elements of H_2 are

$$\langle n-1,-|H_2|n,+\rangle=-\frac{i\gamma}{4}\left[\frac{2eBn}{\hbar}\right]^{3/2} \tag{A18a}$$

and

$$\langle n+3,-|H_2|n,+\rangle=\frac{i\gamma}{4}\left[\frac{2eB}{\hbar}\right]^{3/2}\sqrt{(n+1)(n+2)(n+3)}\ . \tag{A18b}$$

We are interested in the Landau level n that is close to the Fermi level E_F so that $E_F\simeq\varepsilon_1+n\hbar\omega_c$. We then have

$$\frac{2eBn}{\hbar}\simeq\frac{2m^*(E_F-\varepsilon_1)}{\hbar^2}=k_F^2 \tag{A19}$$

where k_F is the Fermi wave vector. Using Eq. (A19) we can write the nonzero matrix elements as

$$\langle n-1,-|(H_1+H_2)|n,+\rangle=i\Delta_I\ , \tag{A20a}$$

$$\langle n+3,-|(H_1+H_2)|n,+1\rangle=i\Delta_{I'}\ , \tag{A20b}$$

where

$$\Delta_I=\gamma K^2 k_F-(\gamma k_F^3/4)\ , \tag{A21a}$$

$$\Delta_{I'}\simeq\gamma k_F^3/4\ \ \text{(for large } n)\ . \tag{A21b}$$

We consider next the effect of the Rashba term [Eq. (4)] which can be written as

$$H_R=\eta(\sigma_x k_y-\sigma_y k_x)\ . \tag{A22}$$

We need to evaluate the matrix elements $\langle\alpha,n,s|H_R|\alpha',n',s'\rangle$ due to H_R between the eigenstates of H_0. Following the previous procedure and expressing H_R in terms of the creation and annihilation operators, we obtain

$$H_R=\eta\left[\frac{2eB}{\hbar}\right]^{1/2}\begin{bmatrix}0 & a\\ a^\dagger & 0\end{bmatrix}\ . \tag{A23}$$

The only nonzero matrix elements of H_R are

$$\langle n-1,+|H_R|n,-\rangle=\Delta_R \tag{A24}$$

where [using Eq. (A19)]

$$\Delta_R=\eta k_F\ . \tag{A25}$$

APPENDIX B: EFFECT OF NONPARABOLIC TERMS

In this appendix, we discuss the effects of the nonparabolic terms that were not included in the Hamiltonian in Eq. (1). The Hamiltonian of the conduction band in the presence of a magnetic field can be expanded in a series of products of irreducible tensor components $\Gamma_l^{(k,\lambda)}$ and a set of 2×2 matrices $X_l^{(k,\lambda)}$ (Ref. 2)

$$H=\sum_{k,\lambda}a_{k,\lambda}\sum_l X_l^{(k,\lambda)}\Gamma_l^{(k,\lambda)} \tag{B1}$$

where $X_l^{(1)}=I_2$, a 2×2 identity matrix, and $X_l^{(4)}\in\{\sigma_l|l=x,y,z\}$, the Pauli spin matrices. Following Ref. 2, Eq. (B1) can be expanded in the form (up to fourth powers of k_x, k_y, k_z)

$$\begin{aligned}H=&a_{11}+a_{12}k^2+a_{13}k^4+a_{14}([k_y^2,k_z^2]+[k_z^2,k_x^2]+[k_x^2,k_y^2])+a_{15}B^2+a_{41}\mu_B\boldsymbol{\sigma}\cdot\mathbf{B}\\&+a_{42}\boldsymbol{\sigma}\cdot\boldsymbol{\kappa}+a_{43}\boldsymbol{\sigma}\cdot\mathbf{B}k^2+a_{44}[\boldsymbol{\sigma}\cdot\mathbf{k},\mathbf{B}\cdot\mathbf{k}]+a_{45}(\sigma_xB_xk_x^2+\sigma_yB_yk_y^2+\sigma_zB_zk_z^2)+a_{46}(\boldsymbol{\sigma}\times\mathbf{k})\cdot\hat{\mathbf{z}}\end{aligned} \tag{B2}$$

where the symbol $[a,b]$ denotes $\frac{1}{2}(ab+ba)$ and the vector $\boldsymbol{\kappa}$ is given by Eqs. (A1) in Appendix A. In the above equation, a_{11} is the reference conduction-band energy at $k=0$. a_{13} and a_{14} are the coefficients for isotropic and anisotropic k^4 nonparabolicity and are responsible for unequal spacing of Landau levels. a_{15} represents a diamagnetic shift in energy. a_{41} is the bulk g factor, and a_{42} is the coefficient of the inversion-asymmetry spin-splitting term. a_{43} represents the isotropic k-dependent contribution to g factor whereas a_{44} and a_{45} represent anisotropic k-dependent contributions to g factor. a_{46} is the spin-orbit-coupling constant. Noting that $a_{42}=\gamma$ in Eq. (3) and $a_{46}=\eta$ in Eq. (4), we can rewrite Eq. (B2) as

$$H=H_0+H_I+H_R+a_{15}B^2+H_{\rm np}+H_{ig}+H_{ag} \tag{B3}$$

where H_0, H_I, and H_R are given by Eqs. (2)–(4). $H_{\rm np}$ represents the nonparabolic terms with coefficient a_{13} and a_{14}. H_{ig} represents the isotropic k-dependent contribution to g factor (coefficient a_{43}) and H_{ag} represents the anisotropic k-dependent contribution to g factor (coefficients a_{44} and a_{45}). In our analysis we have used only the first three terms in Eq. (B3). The other terms were neglected for the following reasons. The term $a_{15}B^2$ becomes important at high magnetic fields, and since the experimental data were at $B<1$ T, this term was neglected. Also, this term does not contribute to spin splitting, $H_{\rm np}$ represents the k^4 nonparabolic terms and is responsible for unequal spacings of the Landau levels. $H_{\rm np}$ is not spin dependent and does not contribute to spin splitting and can be ignored for the present analysis. H_{ig} represents the term with isotropic k-dependent contributions to g factor and is spin dependent. In ESR measurements this term is responsible for the nonlinear behavior of spin splitting with magnetic field.[2] In Ref. 5, the spin splitting is obtained from SdH measurements, and the following discussion shows that we do not expect any nonlinear behavior in the spin splitting from this term. The contributions from the bulk g factor (a_{41}) and a_{43} term can be combined to give

$$H_{gg'}=a_{41}\mu_B\boldsymbol{\sigma}\cdot\mathbf{B}+a_{43}\boldsymbol{\sigma}\cdot\mathbf{B}k^2\ . \tag{B4}$$

Noting that $a_{41}=g$, Eq. (B4) can be expressed as

$$H_{gg'}=g\mu_B\boldsymbol{\sigma}\cdot\mathbf{B}+\boldsymbol{\sigma}\cdot\mathbf{B}a_{43}(k_x^2+k_y^2+k_z^2)\ . \tag{B5}$$

To find the effect of $H_{gg'}$ we need to evaluate its matrix element between the eigenstates of H_0. Following the procedure in Appendix A, restricting to the lowest subband, and noting that $a^\dagger a=n$, we get

$$H_{gg'}=\boldsymbol{\sigma}\cdot\mathbf{B}\left[g\mu_B+a_{43}K^2+a_{43}\frac{2eB}{\hbar}(n+\tfrac{1}{2})\right] \tag{B6}$$

where K^2 [Eq. (A12)] is a measure of the kinetic energy in the z direction due to surface confinement. In ESR measurements, the spin splitting of a fixed Landau level is measured as a function of magnetic field. With n fixed, the last term in Eq. (B6) is proportional to B, and causes the spin splitting to be nonlinear with the magnetic field. In the experiment in Ref. 5 (SdH measurements), n changes with magnetic field and from Eq. (A19) in Appendix A, $2eBn/\hbar=k_F^2$. Hence, the last term in Eq. (B6) is constant with magnetic field and we do not expect any nonlinear behavior in the spin splitting from this term. This term, however, introduces some corrections to the g factor. The perpendicular-field data are at low magnetic fields where the spin splitting is insensitive to g factor, and hence is not affected by this term. Neglecting H_{ig} may, however, introduce some errors in the estimation of g factor in Sec. III. From similar arguments to those above, we have also decided to ignore the anisotropic contributions to g factor (coefficients a_{44} and a_{45}) in our analysis.

[1]D. Stein, K. v. Klitzing, and G. Weimann, Phys. Rev. Lett. **51**, 130 (1983).

[2]G. Lommer, F. Malcher, and U. Rössler, Phys. Rev. B **32**, 6965 (1985).

[3]M. Dobers, K. v. Klitzing, and G. Weimann, Phys. Rev. B **38**, 5453 (1988).

[4]J. Luo, H. Munekata, F. F. Fang, and P. J. Stiles, Phys. Rev. B **38**, 10 142 (1988).

[5]B. Das, D. C. Miller, S. Datta, R. Reifenberger, W. P. Hong, P. K. Bhattacharya, J. Singh, and M. Jaffe, Phys. Rev. B **39**, 1411 (1989).

[6]B. Das, Ph.D. thesis, Purdue University, West Lafayette, IN,

May, 1989.
[7]W. P. Hong, G. I. Ng, P. K. Bhattacharaya, D. Pavlidis, S. Willing, and B. Das, J. Appl. Phys. **64**, 1945 (1988).
[8]R. Eppenga and M. F. H. Schuurmans, Phys. Rev. B **37**, 10923 (1988).
[9]L. M. Roth, Phys. Rev. **173**, 755 (1968).
[10]C. R. Whitsett, Phys. Rev. **138**, A829 (1965); M. M. Miller and R. Reifenberger, Phys. Rev. B **38**, 3423 (1988); D. G. Seiler, W. M. Becker, and L. M. Roth, *ibid.* **1**, 764 (1970); D. G. Seiler, B. D. Bajaj, and A. E. Stevens, *ibid.* **16**, 2822 (1977).
[11]G. Lommer, F. Malcher, and U. Rössler, Phys. Rev. Lett. **60**, 728 (1988).
[12]Y. A. Bychkov and E. I. Rashba, J. Phys. C **17**, 6039 (1984); in *Proceedings of the 17th International Conference on the Physics of Semiconductors, 1984,* edited by J. D. Chadi and W. A. Harrison (Springer-Verlag, Berlin, 1984), p. 321.
[13]M. S. Lundstrom and R. J. Schuelke, Solid State Electron. **25**, 683 (1982).
[14]S. Adachi, J. Appl. Phys. **53**, 8775 (1982).
[15]B. Wakefield, M. A. G. Hallimell, T. Kerr, D. A. Andrews, G. J. Davies, and D. R. Wood, Appl. Phys. Lett. **44**, 341 (1984).
[16]D. Olego, T. Y. Chang, E. Silberg, E. A. Caridi, and A. Pinczuk, Appl. Phys. Lett. **41**, 476 (1982).
[17]G. Gregoris, J. Beerens, S. Ben Amor, L. Dmowski, J. C. Portal, D. L. Sivco, and A. Y. Cho, J. Phys. C **20**, 425 (1987).
[18]R. People, K. W. Wecht, K. Alavi, and A. Y. Cho, Appl. Phys. Lett. **43**, 118 (1983).
[19]M. J. McLennan, M. S. thesis, Purdue University, West Lafayette, IN, May, 1987.
[20]R. J. Nicholas, M. A. Brummell, J. C. Portal, A. Y. Cho, K. Y. Cheng, and T. P. Pearsall, in *Proceedings of the Conference on Application of High Magnetic Fields in Semiconductor Physics, Grenoble, 1982,* Vol. 177 of *Lecture Notes in Physics* (Springer-Verlag, Berlin, 1983), p. 110.
[21]F. F. Fang and P. J. Stiles, Phys. Rev. **174**, 823 (1968).
[22]M. Braun and U. Rössler, J. Phys. C **18**, 3365 (1985).
[23]Sudha Gopalan, J. K. Furdyna, and S. Rodriguez, Phys. Rev. B **32**, 903 (1985).